# Triggering of the 2012 Ahar-Varzaghan earthquake doublet (Mw6.5&6.3) by the Sahand Volcano and North Tabriz fault (NW-Iran); Implications on the seismic hazard of Tabriz city

**Seyyedmaalek Momeni**[1,2*]

1. EPFL Geo-Energy Lab – Gaznat Chair on Geo-Energy, EPFL-ENAC-IIC-GEL, Station 18, CH-1015, Lausanne, Switzerland.

2. International Centre for Theoretical Physics (ICTP), Trieste, Italy.

***** Corresponding author, E-mail: maalek.momeni@gmail.com

**Abstract**

Seismic history of the North Tabriz fault (NTF), the main active fault of Northwestern Iran near Tabriz city, and its relation to the Sahand active Volcano (SND), the second high mountain of the NW Iran, and to the 11 August 2012 Ahar-Varzaghan earthquake doublet (Mw6.5&6.3) (AVD), is investigated. I infer that before AVD seismicity of the central segment of NTF close to SND was very low compared to its neighbor segments. Magmatic activities and thermal springs near central NTF close to Bostan-Abad city and low-velocity anomalies reported beneath SND toward NTF in tomography studies suggest that the existing heat due to SND magma chamber has increased the pore-fluid pressure that overcomes the effective normal stress on the central NTF, resulting in its creep behaviour. Two peaks of cumulative scalar seismic moments of earthquakes observed on both lobes of the creeping segment, confirming the strong difference in the deformation rate between these segments. On 2012, AVD struck in the 50 km North of NTF, in the same longitude range to SND and with the same right-lateral strike-slip mechanism to

NTF, as a result of partial transfer of the right-lateral deformation of NW Iran toward the North of NTF on the Ahar-Varzaghan fault system. A cumulative aseismic slip equal to an Mw6.8 event is estimated for the creeping segment of NTF, posing half of the 7mmy-1 geodetic deformation has happened in the creep mode. This event has transferred a positive Coulomb stress field of >1 bar on the AVD and triggered them. Also, the western and eastern NTF segments received >4 bar of positive Coulomb stresses from the creeping segment and are probable nucleation locations for future earthquakes on NTF. The observed creep may be the reason for the NTF segmentation during the 1721AD M7.6 and 1780 AD M7.4 historical earthquakes.

**Keywords:** Induced seismicity; aseismic deformation; pore-fluid pressure; effective stress; volcano; triggering

## 1. Introduction

On 11 August 2012, an earthquake doublet with Mw6.5 and Mw6.3 occurred in NW Iran near the Ahar and Varzaghan cities (AVD), 40 km Northeast of Tabriz city (TBZ), the fourth megacity of Iran with >2 million population. They located in 50 km North of Sahand Volcano (SND), which situated 40 km Southeast of TBZ. AVD caused >300 fatalities. In terms of mechanism, the first mainshock exhibits an almost pure right-lateral strike-slip faulting, and the second one had two slip patches with right-lateral strike-slip and reverse mechanisms (Fig. 1a, Momeni & Tatar, 2018; Momeni et al, 2019). The first mainshock produces almost 12 km of surface rupture. The mainshocks mechanisms and their rupture geometries were almost the same to the North Tabriz Fault (NTF), the main active fault of northwestern Iran, that crosses just

47 North of TBZ. Before AVD, the seismicity on the Ahar-Varzaghan fault system was negligible,
48 so that these events were a surprise in that region.
49
50 **1.1. Tectonic Settings**
51 NW of Iran is a part of Turkish-Iranian plateau, bounded by the Caucasus Mountains to the
52 North, Zagros Fold and thrust belt to the South, and Talesh Mountains to the East. This region is
53 under complex tectonics which resulted in high deformation and seismic activity (Berberian and
54 Arshadi, 1976; Jackson, 1992; Ghods et al., 2015; Momeni & Tatar, 2018) (Fig. 1). The main
55 tectonic regime is the oblique convergence of Arabia-Eurasia with the current deformation rate
56 of about 13–15 mmy−1, at the longitude of 46.1 °E (Vernant et al., 2004; Reilinger et al., 2006).
57 The Talesh Mountains on the eastern termination of the region is either colliding to the relatively
58 thick South Caspian sedimentary cover (~20 km) (Zamani and Masson, 2014) or, the South
59 Caspian crust is under-thrusting westward beneath it (Jackson et al., 2002). Two different
60 northeastward and northwestward deformation directions are observable in the GPS velocity
61 vectors at the longitude of 44°E, which suggest it as the western margin of the region (Momeni
62 & Tatar, 2018).
63
64 Earthquakes mechanisms (GCMT) and surface deformation studies (Reilinger et al., 2006;
65 Djamour et al., 2011) suggest the resulting deformation in NW Iran is mainly the right-lateral
66 strike-slip faulting on the W-NW striking faults within the region. While thrust faulting is
67 partitioned to the North on the Great Caucasus (Jackson, 1992; McClusky et al., 2000; Momeni
68 & Tatar, 2018). The two N-S to NE- SW (N018°) shortening and NW-SE (N287° and N155°)
69 strike-slip deformation stress regimes were obtained by Zamani and Masson, (2014). The first

stress system developed the three E-W striking fold and thrust belts, Arasbaran, Ghoshe-dagh and Bozkosh mountain ranges. While the N-S striking structures like Talesh mountains corresponds to the second stress system (Fig. 1a).

NTF with the main right-lateral strike-slip mechanism and deformation rate of 7 ± 1 mmy−1 accommodates most of the deformation of the region (Djamour et al., 2011). Rizza et al., (2013) estimated that the current deformation rate has been mostly constant since late quaternary until now (during the past 45 ka). However, they remarked a decrease in the strike-slip deformation rates along the NTF from about 7 mmy−1 to 5 mmy−1 from the West to the East of 47° longitude, and they relate it to the fault orientation changes from about NW-SE to W-E (Djamour et al., 2011; Rizza et al., 2013) (Fig. 2a). Later, Su et al., (2017) reported subsidence in the closest GPS station to the Northeast SND near BA and interpreted it as magmatic activities of Sahand.

A microseismicity study along the NTF using a local seismic network confirmed the main shear deformation mechanism of NTF in the upper crust (Moradi et al. 2011). On the western and eastern terminations of NTF, the North Mishu Fault (NMF) and the South Bozkosh Fault (SBF) are the two oblique reverse faults with right-lateral strike-slip components that strike ~E-W and dip to the South and North, respectively. Solaymani Azad et al., (2015) called the NTF, NMF, and SBF as Tabriz Fault System (TFS).

Before the occurrence of the 2012 earthquake doublet, the Ahar-Varzaghan fault system has been in a long seismic quiescence (Momeni & Tatar, 2018; Fig. 1a). However, field observations revealed the continuation of fault to the both East and West of the ruptured segment during the

2012 AVD (e.g. Copley et al. 2013, Donner et al. 2015, Ghods et al. 2015). The clear segmentation has been observed along this fault system with different kinematics and without clear connections that suggest it as a young fault system (Donner et al., 2015). The occurrence of the AVD suggested that some of the shear strain of the region is not compensating by the NTF, specifically at the longitudes east of 46°E (Donner et al. 2015; Ghods et al. 2015).

Sahand volcano with 3707 m elevation is an isolated, extensively distributed (~3000 km2 area) stratovolcanic complex (Ghalamghash et al., 2019). Together with Sabalan and Saray, they are three Late Miocene-Quaternary volcanoes that formed as results of the collision between the Arabian and Eurasian plates along the Neo-Tethyan suture zone in NW Iran. The formation of Neo-Sahand is estimated to ca. 600 to b173 ka (Ghalamghash et al., 2019). They mostly observed within and outside of the widely eroded caldera margin. Neo-Sahand units include basaltic andesitic to rhyolitic domes in the center of the complex as well as small parasitic cones along with subvolcanic dikes toward the northeast.

### 1.2. Historical earthquakes of NW Iran

Historical seismicity is widely distributed in the region, and mostly on the NTF and NMF. Tabriz city has been the capital of Iran and Azerbaijan in the past. Several large destructive historical earthquakes (magnitudes up to Ms=7.6) have reported for Tabriz (Ambraseys and Melville, 1982; Berberian and Yeats, 1999). Most of them are related to the activity of NTF (Fig. 1a). The last two M>7 destructive historical earthquakes have occurred on 1721 AD and 1780 AD, that ruptured more than 50 km of the southeastern and northwestern segments of the NTF and caused

115 over 40,000 and 200,000 fatalities, respectively (Ambraseys and Melville, 1982; Berberian and
116 Yeats, 1999; Momeni & Tatar, 2018).
117
118 Paleoseismological studies revealed at least three major (M~7.5) historical earthquakes for the
119 southeastern segment over the past 33.5 ka, including the 1721 AD M7.6–7.7 earthquake
120 (Solaymani Azad et al., 2015). On the other side, four historical earthquakes are reported for the
121 northwestern segment of the NTF during the past 3.6 ka, the most recent being the Ms~7.4 1780
122 AD earthquake (Hessami Azar et al., 2003). The estimated slip per event and slip rate on this
123 segment are 4 ± 0.5 m and 3.1–6.4 mmy−1, respectively, and the average recurrence interval of
124 large earthquakes on it is estimated in the range of 350 to 1430 years.
125 NMF and SBF also ruptured during historical earthquakes, the last two being the 1786 AD
126 Marand and 1593 AD Sarab earthquakes that suggest a seismic migration from the southeast
127 toward the northwest of TFS. They also reveal earthquake clustering (e.g. Kagan and Jackson,
128 1991; Berberian, 1997; Karakhanian et al., 2004) and interaction between fault segments of the
129 TFS (Solaymani Azad et al., 2015).
130
131 **1.3. <u>Instrumental earthquakes of NW Iran</u>**
132 Mechanism of deformation strongly changes from the western Alborz to the Iran-Turkey
133 borders. The 1976 Mw7.0 Chalderan earthquake has occurred near the borders of Iran with
134 Turkey on the right-lateral strike-slip Chalderan-Khoy fault that strikes E-W. While, the 1990
135 Mw7.4 Rudbar-Tarom earthquake on the western Alborz mountains has occurred on a left-lateral
136 strike-slip fault trending WNW- ESE (Momeni & Tatar, 2018).

Within the NW Iran before the AVD, the 1997 Mw = 6.1 Ardebil earthquake occurred on an N-S striking fault situated ~150 km East of the AVD, showing a pure left-lateral strike-slip faulting (Aziz Zanjani et al., 2013). On 11 August 2012, the AVD occurred that were very well recorded by different instruments. The first mainshock with Mw6.5 had a right-lateral strike-slip mechanism. While the second one with Mw6.3 was more complex and contained two slip patches: the first patch had a right-lateral strike-slip mechanism, and the second one had a reverse mechanism (Momeni et al., 2019). The last large earthquake in the region is the 7 November 2019 Mw5.9 Torkamanchay earthquake (TKC) that occurred on an NE striking left-lateral strike-slip fault between North and South Bozkosh Faults (Valerio et al., 2020).

The EHB catalog (Engdahl et al., 2006) shows most of the seismicity on the Talesh mountains and also on the NMF (Fig. 1a). However, no large earthquake (M>5) reported on the segments of NTF in the GCMT catalog (Fig. 1b).

In 1995 a local permanent seismic network consisting of eight stations, known as Tabriz sub-network of the Iranian Seismological Center (IRSC), was installed in the region (Fig. 1b). However, this sparse network (station spacing ~50 km) limited the number of precisely located earthquakes. There are only 70 earthquakes in IRSC catalog from 1995 until the end of 2005, and none of them has located close (distance <5km) to NTF. From 2006, after the installation of the Broadband Iranian Network (BIN) maintained by the International Institute of Earthquake Engineering and Seismology (IIEES) in Tehran, Iran, and improvement of IRSC network data, the IRSC locations improved in terms of accuracy and magnitude completeness.

159 Figure 1b shows the precisely located seismicity of the region recorded in the IRSC network
160 from 1995 until the occurrence of AVD in August 2012. They have located by at least five
161 stations, have a location error of <5 km, RMS of <0.5 s, and azimuthal gap of <270°. They are
162 all smaller than Mw5.0 unless the 1997 Ardabil earthquake. They mostly have shallow focal
163 depths (< 20 km) and are distributed mainly along the NTF and NMF. However, the central
164 segment of NTF near SND shows much lower seismic activity compared to the western and
165 eastern segments (Fig. 1b). A seismic cluster on the North of AVD is mainly related to mining
166 activities in that area. The rest of the seismicity is related to the Astaneh (ASF), West Alborz
167 (WAF), South Qoshadagh (SQF), Goshachay (GCF), South Bozkosh (SBF), North Mishu
168 (NMF), Maragheh (MGF), Khajeh (KHF), and Nehram (NHF) faults. After AVD, the only large
169 event of the region is the 7 November 2019 Mw5.9 Torkamanchay earthquake that occurred on
170 an NE striking vertical dip fault between NBF and SBF near the eastern termination of NTF.
171 Detailed microseismic monitoring on the NTF by a local dense seismic network data confirmed
172 its right-lateral strike-slip mechanism with an East-Southeastward oriented fault plane (Moradi et
173 al., 2011; Fig. 4). Microearthquakes located by Moradi et al., (2011) on NTF situated in the
174 upper crystalline crust at depths shallower than 20 km. Moradi et al. proposed a vertical dip fault
175 plane for the NTF.
176

177 **1.4. <u>The goal</u>**

178 In this study, the seismic activity of the NTF from historical earthquakes until 2020 is
179 investigated. A cumulative slip model has proposed for the creeping segment of NTF near SND,
180 and, the transferred Coulomb stress by this aseismic deformation on the AVD ruptures has
181 computed. Ultimately, the relation between NTF seismic-aseismic deformation activity to SND

and AVD, and changes in the rheology of the central segment of NTF near SND after AVD investigated.

## 2. Seismicity along NTF and NMF

As mentioned before, earthquake locations by IRSC seismic network in NW Iran started in 1995. However, the IRSC catalog is poor until the end of 2005 due to data quality and sparsely distanced stations (>50 km). There are no earthquakes in the distance of 5 km to the NTF from 1995 to the end of 2005. From 2006, earthquake monitoring has improved in this region in terms of location accuracy and magnitude completeness.

The well-located earthquakes in the distance of 5 km to NTF and NMF are selected from 2006 until before the AVD and from AVD until November 2019 TKC in the IRSC network. These sets are recorded in >=5 stations, with location errors of <5 km, RMS of <0.5 s, and azimuthal gap of < 270°. The first set contains 512 earthquakes in which 45 of them have magnitudes 2.5 and higher. I infer that the central segment of NTF near SND has a long quiescence from 2006 until the occurrence of AVD. However, the two nearby segments show high seismicity (Fig. 2a). After AVD, 69 M>=2.5 earthquakes are in 5 km distance to NTF and NMF (IRSC catalog) with a distributed seismicity and their most concentration on the NMF (Fig. 2b; Table S3). However, the two relatively large events (3.7<M<4.0) are located in the central NTF near SND (Fig. 2b).

The cumulative scalar seismic moments of the earthquakes that occurred after 2006 until the 2012 AVD, and after that until TKC, is computed to investigate the seismic energy release behaviour along the NTF and NMF. The cumulative scalar seismic moment plot of the first set shows two peaks in the Eastern and Western lobes of central NTF that matches to SND, and one on the NMF (Fig. 2b). However, the central NTF itself was almost silent.

For earthquakes that occurred on NTF After AVD, the cumulative scalar seismic moment plot shows a peak in the middle of the central NTF. However, the previously observed peaks of the scalar seismic moment on its lobes are disappeared (Fig. 2b). There is also a relatively wide peak on the NMF, North of Urmieh Lake, where the high seismicity was also observed before AVD.

## 3. Creeping segment of NTF near SND

Creeping behaviour is mainly related to frictional strength of the fault zone material, depending on lithology, temperature, and pore-fluid pressure (i.e. Avouac, 2015, Khoshmanesh & Shirzaei, 2018). The magmatic activities reported in a GPS study by Su et al., (2017) near BA, known thermal springs there, and absence of seismic activity from 2006 until 2012 AVD on the central NTF near BA, propose that the existing heat due to the SND magma chamber decrease the effective normal stress on this segment of the fault by increasing the pore-fluid pressure on the fractured fault area and consequently cause it to creep. The resulting different deformation rates along NTF segments is probably the reason for the observed two peaks of high cumulative scalar seismic moments on both lobes of central segment of NTF near SND.

To prove this idea, a cumulative aseismic deformation on the central segment of NTF is estimated. This segment didn't rupture since the 1721 M7.6 historical earthquake and the GPS study by Djamour et al., (2011) and Rizza et al., (2013) suggest right-lateral deformation of 7mmy-1 for this segment. A maximum slip of 0.007*(2012-1721) =2.04 meters is expected for this segment until the AVD. This segment has a strike/dip of 300°/90° and covers the silent central segment of NTF with a length of ~30 km and locking depth of ~20 km that is suggested by Djamour et al., (2011). I stress that Rizza et al., (2013) suggested a relatively unchanged

deformation rate on NTF since 65 ka. If I fairly pose that only half of this deformation has happened in creep mode and the other half is locked (and may rupture in a future earthquake), the slip model will have a maximum value equal to 1.02 m. Later in section 4, I will explain that even considering the smaller contribution of creep in the whole deformation (i.e. 25%), the transferred stress field by the creeping segment will be high enough to trigger the AVD. An elliptical slip patch (i.e. Ruiz & Madariaga, 2013; Momeni et al., 2019) is proposed with a max slip of 1.02 m at the center and with a Gaussian distribution of slip and half of the max slip equal to ~51 cm on the borders, where high seismic activity is observed (Fig. 2a). The resulting source has a scalar seismic moment of ~2.0*e+19 Nm equal to an Mw6.8 earthquake. For a fully creeping slip model, the source will have a scalar seismic moment of ~4.0*e+19 Nm equal to an Mw7.0 earthquake.

The resulting deformation may transfer positive Coulomb failure stresses on the nearby faults. I note that AVD has occurred in the same longitude to this creeping segment, suggesting that the right-lateral deformation does not fully release on NTF and probably some of it transfer toward North, as also suggested by Donner et al., (2015) by geological investigations.

## 4. Stress transfer

### 4.1. Stress transfer from the creeping segment of NTF to AVD

The stress tensor produced by the defined slip model for the creeping segment of NTF is calculated on a 3-D grid in the region using a method by Wang et al. (2003) (Fig. 3). The method is based on the dislocation theory that is implemented in a multilayered media. A 1-D crustal velocity model of the area retrieved from precisely located aftershocks of AVD is used, and a

Poisson ratio of ~0.25 obtained from a Vp/Vs ratio of 1.74 (Momeni & Tatar 2018, Table S1). The Coulomb stress field is calculated on optimally oriented ruptures of both Ahar-Varzaghan earthquakes, and by considering strike-slip mechanisms of their slip patches obtained by Momeni et al., (2019).

A positive Coulomb stress of >1 bar is transferred from the creeping segment on the ruptured areas during the doublet (Fig. 3a). Also, the creeping segment had positive coulomb stress transfer of >4 bar on the nearby segments and excited them to slip (Fig. 3b), especially on the western segment of NTF (e.g., Vadacca, 2020).

### 4.2. Stress transfer from AVD to NTF

The stress tensor produced by the AVD ruptures that were obtained in a study by Momeni et al., (2019) is computed on the region using the same method mentioned in section 4.1. As was also reported by Momeni et al., (2019), the stress field shows a positive Coulomb stress transfer of >0.1 bar on most of the creeping segment of NTF, and also ~0.1 bar on the NBF (Fig. 4a). The two peaks of cumulative scalar seismic moments of earthquakes are observed in these segments on NTF and NBF from the 2012 AVD until the 2019 TKC (Fig. 2b).

A cumulative positive normal stress transfer of >0.1 bar is obtained from AVD on most of the creeping segment of NTF (Fig. 4b). This additional positive normal stress to the regional stress may increase the effective normal stress on the creeping segment and change its rheology from partial creep to more stick-slip. The occurrence of two earthquakes on the proposed creep segment after the AVD which is also observed as a peak of the scalar seismic moment in Figure 2d confirms our suggestion.

On the NMF, two a wide peak of the cumulative scalar seismic moment was observed North of Urmieh Lake before AVD. While after the doublet, there is a peak of the cumulative scalar seismic moment in between of the previous wide peak suggesting that this part was partially locked, and has been excited by the doublet. Also, these seismic activities may be partly related to the relatively higher pore-fluid pressure provided by the Urmieh Lake on the NMF, or by the recent dramatic decrease of 90% of the water volume of the lake during years 1995 to 2013 (Schulz et al., 2020) that may reduce the effective normal stress on NMF, unclamp it, and excite it to slip.

## 5. Discussion

The seismicity of the NTF and NMF is investigated from documented historical earthquakes to November 2019 TKC earthquake. Many historical earthquakes are referred to NTF (Fig. 1a). The last two historical earthquakes of 1721 AD and 1780 AD cover all NTF segments. EHB catalog shows most of the seismic activity on the western termination of NTF. However, the GCMT catalog does not have any earthquake on the NTF.

The IRSC network earthquake catalog has improved from 2006 in terms of completeness and location accuracy. There are 512 earthquakes (45 of which have Ml>=2.5; Table S2) in the distance of 5 km from NTF and NMF for a period from 2006 until before AVD. These seismic activities are distributed along all segments of NTF and NMF unless the central segment of NTF that is situated North of SND and shows much less seismicity compared to its neighbor segments. Two remarkable peaks are observable in the cumulative scalar seismic moments of these earthquakes on both lobes of the central segment of NTF near SND (Figure 2b). A

297 probable explanation for such behaviour is that the segment of NTF near SND is partially
298 creeping. Djamour et al., (2011) and Rizza et al., (2013) reported a decrease in right-lateral
299 surface deformation rate from West of BA (Longitude 47°) to the East from 7mmy-1 to 5mmy-1.
300 Su et al., (2017) remarked that the region near BA is affected by deep magmatic activities of
301 SND. This segment is close to the thermal areas (hot springs) near BA reported by Ghalamghash
302 et al. (2019). Tomography studies by Rezaeifar et al., (2016) and Bavali et al., (2016) revealed a
303 heterogeneous structure in this region with high and low-velocity anomalies. A low-velocity
304 region has obtained beneath SND at depths deeper than 8 km that extends until the NTF by
305 Bavali et al., (2016) (Fig. 5). However, at shallower depths, a relatively high-velocity anomaly
306 obtained by Rezaeifar et al., (2016), and interpreted as cooled magmatic rocks of SND. The
307 observed thermal activities near BA area are probably due to the existence of some dyke-like
308 branches of the SND deep magma chamber in that area that was also suggested by Ghalamghash
309 et al. (2019) as many young craters with dacitic to rhyolitic parasitic cones of magma of neo-
310 Sahand were observed toward NNE of SND near BA (see Fig. 3). The other explanation will be
311 the possible aid of NTF fractured area which is extended down to the depth of 20 km, in bringing
312 heat to the surface. The existing heat increases the pore-fluid pressure in the fault area and
313 unclamps this segment of NTF, facilitating its creep.
314
315 However, this segment of NTF was ruptured as a part of the 1721 AD M7.6 earthquake. Harris,
316 (2017) mentioned that the creeping segments are also potential to rupture in M~6.8 earthquakes,
317 and they usually rupture together with their nearby segments (i.e. Van den Ende et al., 2020).
318 Dynamic weakening is the probable mechanism for rupture of such fault segments (i.e. Noda &
319 Lapusta, 2013). The same mechanism may have happened during the 1721 AD earthquake, and

that is most likely the reason for segmentation of NTF during 1721 AD and 1780 AD historical earthquakes.

The effect of raise of pore-fluid pressure in facilitating the fault creep/slip is widely observed and reported mostly for Strike-slip faulting mechanism (e.g. Avouac, 2015, Floyd et al., 2016, Goebel et al., 2017, Scuderi et al., 2017, Michel et al., 2018, Johann et al., 2018, Eaton & Schultz, 2018, Zhu et al., 2020, Momeni & Madariaga, 2020).

A slip model is estimated for the creeping segment of NTF from 1721 AD until before the 2012 AVD considering that half of the 7 mmy-1 right-lateral deformation rate obtained by Djamour et al., (2011) and Rizza et al., (2013) was happening in creep mode. This creep has occurred at the longitudes between 46.55° E to 46.85° E and with a locking depth of 20 km. Having a maximum cumulative slip of 1.02m, the obtained cumulative scalar seismic moment is 2.0 * e+19 Nm equal to Mw6.8 (for the fully creep mode, this value raises to 4.0 * e+19 Nm equal to Mw7.0). This also remarks that the other segments of NTF have a considerable amount of accumulated tectonic stress.

The creeping segment of NTF transferred positive Coulomb stress field of >4 bar on the neighbor segments, and brought them closer to failure (Fig. 3b). That is confirmed by the observation of two peaks of cumulative scalar seismic moments on both lobes of the creeping segment. These earthquakes can be considered as aftershocks of the creep event. Aftershocks surrounding a slip model is a consistent feature of large earthquakes (see Henry & Das, 2002).

343 The 3D stress field produced by this creep source on AVD is computed. The estimated slip
344 model for the creeping segment can transfer positive Coulomb stress of >1 bar on the AVD and
345 trigger them (Fig. 6). After the AVD until November 2019, one peak of the cumulative scalar
346 seismic moment is observed for earthquakes occurred in 5 km distance from NTF, and that is in
347 the middle of the central NTF. There is also one peak on the NMF. Observation of seismic
348 activity on the previously creeping segment of NTF and absence of two peaks of cumulative
349 scalar seismic moments on both lobes of that segment suggest a change in its rheology from
350 creep to stick-slip after AVD. This change is probably due to the positive static normal stress
351 field of >0.1 bar that was transferred from AVD on half of the creeping segment of NTF. Also,
352 Momeni et al., (2019) compute the stress field by AVD on NTF and NMF and reported transfer
353 of positive Coulomb stress of >0.1 bar on the central segment of NTF as well as NMF. For the
354 NMF, two relatively small peaks of cumulative scalar seismic moment release are observed
355 before the AVD (Fig. 2b). After AVD, one big peak is observed in between the two previous
356 peaks suggesting that this part of NMF was partially locked, and triggered by the 2012 AVD.
357
358 Seismic quiescence of the creeping segment of NTF near SND from 2006 together with the
359 observed magmatic activities in that area proposes a strong relation between the volcanic activity
360 of SND and frictional properties of that segment of NTF. Compared to the central NTF, the
361 western segment that is closer to the Tabriz city shows higher seismic activity. Also, the Eastern
362 segment shows considerable seismic activity which highlights its importance as another potential
363 segment of the NTF for future large earthquakes.
364

The smooth geometry of the central and western segments of NTF may facilitate the rupture expansion on them. However, low seismic coupling in the creeping central NTF may act as a barrier and stop ruptures from expansion toward the western segment.

The suggested 20km thick seismogenic layer for NTF (Djamour et al., 2011; Moradi et al. 2011), highlights its potential for the production of large earthquakes and with low-frequency seismic energy contents that can reach to Tabriz city with less damped energy and affect the tall buildings.

## 6. Conclusion

I infer a seismic quiescence in the central segment of the NTF, North of SND from 2006 until August 2012 AVD. While the two eastern and western segments of NTF show much higher seismicity with two remarkable peaks of cumulative scalar seismic moments on both lobes of the central segment near SND. The existing heat by the SND magma chamber near the fractured area of central NTF raises the pore-fluid pressure and decreases the effective normal stress there, consequently unclamp the fault, and facilitate the right-lateral creep. An Mw6.8 half-creep slip model is suggested for this segment considering half of 7 mmy-1 constant geodetic deformation rate on it since the 1721 AD historical earthquake.

The creeping segment is situated in almost the same longitude range to the 2012 AVD and transferred positive Coulomb stress fields of >1 bar on them. This segment also transferred >4 bar of positive Coulomb stress on its neighbor segments, where the two peaks of cumulative seismic moments were observed. Some of the right-lateral deformation stresses on central NTF

387 transferred to the North and released during the 2012 AVD on the Ahar-Varzaghan complex
388 fault system (Fig. 6).
389
390 After the AVD until TKC, two new peaks of the cumulative scalar seismic moment have
391 observed for earthquakes that occurred on NTF and NMF. One is exactly in the middle of the
392 previously creeping central segment of NTF, consistent to the obtained transfer of positive
393 normal and Coulomb stresses on this segment by AVD (i.e. Momeni et al., 2019). The
394 transferred stress changed the rheology of the creeping segment from mostly creeping to
395 temporary stick-slip.
396 The other peak of the cumulative scalar seismic moment is on the NMF North of Urmieh Lake,
397 and, may be due to the existing pore-fluid pressure or a recent dramatic decline in the water level
398 of the lake over the past two decades (90% decrease in its volume has happened during 1995 to
399 2013; Schulz et al., 2020) that both reduce the effective normal stress on NMF, unclamp it, and
400 facilitate slip on it (e.g. Saar & Manga, 2003).The two peaks of cumulative scalar seismic
401 moments observed before AVD on the western and eastern lobes of the creep segment of NTF
402 near SND were disappeared after AVD until November 2019 TKC, suggesting a change in
403 seismic activity of NTF along its segments by the transferred stress fields produced by AVD, at
404 least for the first 8 years. This change is probably temporary and NTF will return to continue its
405 creep behaviour in the central segment near SND.
406 In terms of rupture dynamics, the two highly stressed neighbor segments of NTF are prone to
407 nucleate earthquakes (e.g. Vadacca et al., 2020). If an earthquake nucleates on the stressed lobes
408 of the creeping segment and its rupture grow toward the West, it will cause a strong directivity
409 effect for that earthquake toward Tabriz city. However, the creeping segment may work as a

410 barrier and probably does not allow NTF to rupture in both Central and Western segments in one
411 larger earthquake.
412
413 The change in seismic activity on the different segments of NTF and having mix behaviour of
414 lock and creep deformation on them raise the seismic hazard in the region, especially for the
415 Tabriz city that currently host > 2 million people. I suggest continuous monitoring of seismicity
416 along NTF will help to understand the rheological behaviours of segments of this mature fault
417 system, with a concentration on the central and western segments that did not rupture in large
418 events since the 1721 AD and 1780 AD historical earthquakes.
419

420 ## 7. Data and Resources

421 The earthquakes data are available through the Iranian Seismological Center (IRSC) network
422 website (http://irsc.ut.ac.ir). The earthquake focal mechanisms in Figure 1b are from the GCMT
423 catalog (http://www.globalcmt.org/CMTsearch.html last access on August, 2020). The
424 supplementary data includes velocity model of the area and earthquakes hypocenters
425 information.
426

427 ## 8. Acknowledgements

428 This research did not receive any specific grant from funding agencies in the public, commercial,
429 or not-for-profit sectors. I thank IRSC and IIEES networks for providing the seismic data.
430 Figures plotted using Generic Mapping Tools (GMT) (http://gmt.soest.hawaii.edu/), Paraview
431 software (https://www.paraview.org), and personal codes in Matlab environment
432 (https://www.mathworks.com).

## 9. References


Ambraseys, N.N. & Melville, C.P., 1982. A History of Persian Earthquakes, Cambridge Univ. Press. https://doi.org/10.1016/j.jseaes.2008.08.001

Avouac, J.P., 2015. From Geodetic Imaging of Seismic and Aseismic Fault Slip to Dynamic Modeling of the Seismic Cycle, Annu. Rev. Earth Planet. Sci. 2015. 43:233–71, doi: 10.1146/annurev-earth-060614-105302.

Aziz Zanjani, A., Ghods, A., Sobouti, F., Bergman, E., Mortezanejad, G., Priestley, K., Madanipour, S., Rezaeian, M., 2013. Seismicity in the western coast of the South Caspian Basin and the Talesh Mountains. Geophys. J. Int. 194, 799–814. https://doi.org/10.1093/gji/ggt299

Bavali, K., Motaghi, K., Sobouti, F., Ghods, A., Abbasi, M., Priestley, K., Mortezanejad, G., Rezaeian, M., 2016. Lithospheric structure beneath NW Iran using regional and teleseismic travel-time tomography, Physics of the Earth and Planetary Interiors 253, 97–107. http://dx.doi.org/10.1016/j.pepi.2016.02.006

Berberian, M., Arshadi, S., 1976. On the evidence of the youngest activity of the North Tabriz Fault and the seismicity of Tabriz city. Geol. Surv. Iran Rep. 39, 397–418.

Berberian, M., 1997, Seismic sources of the Transcaucasian historical earthquakes. In S. Giardini and Balassanian, S. (Eds.), Historical and prehistorical earthquakes in the Caucasus. Kluwer Academic Publishing, Dordrecht, Netherlands, pp. 233–311.

Berberian, M. & Yeats, R.S., 1999. Patterns of historical earthquake rupture in the Iranian Plateau. Bulletin of the Seismological Society of America **89**, 120–139.

Berberian, M. & Yeats, R.S., 2001. Contribution of archaeological data to studies of earthquake history in the Iranian Plateau. Journal of Structural Geology **23**, 563–584.

Copley, A., Faridi, M., Ghorashi, M., Hollingsworth, J., Jackson, J., Nazari, H., Oveisi, B., Talebian, M., 2013. The 2012 August 11 Ahar earthquakes: consequences for tectonics and earthquake hazard in the Turkish-Iranian plateau. Geophys. J. Int. 196, 15–21. http://dx.doi.org/10.1093/gji/ggt379

Djamour, Y., Vernant, P., Nankali, H.R. & Tavakoli, F., 2011. NW Iran eastern Turkey present-dat kinematics: results from the Iranian permanent GPS network, Earth planet. Sci. Lett., 307, 27–34. http://dx.doi.org/10.1016/j.epsl.2011.04.029

Donner, S., Ghods, A., Krauger, F., Roßler, D., Landgraf, A. & Ballato, P., 2015. The Ahar-Varzeghan earthquake doublet (Mw 6.4 and 6.2) of 11 August 2012: regional seismic moment tensors and a seismotectonic interpretation, Bull. seism. Soc. Am., 105, doi:10.1785/0120140042.

Eaton, D.W., & Schultz, R., 2018. Increased likelihood of induced seismicity in highly overpressured shale formations, Geophysical Journal International, 214(1), 751–757, https://doi.org/10.1093/gji/ggy167.

Engdahl, E.R.; Jackson, J.A.; Myers, S.C.; Bergman, E.A.; Priestley, K. Relocation and assessment of seismicity in the Iran region. Geophys. J. Int. 2006, 167, 761–778. http://dx.doi.org/10.1111/j.1365-246X.2006.03127.x

Floyd, M.A., et al., 2016. Spatial variations in fault friction related to lithology from rupture and afterslip of the 2014 South Napa, California, earthquake, Geophys. Res. Lett., 43, doi:10.1002/2016GL069428.

Ghalamghash, J., Schmitt, A.K., Chaharlang, R., 2019. Age and compositional evolution of Sahand volcano in the context of post-collisional magmatism in northwestern Iran: Evidence for

478 time-transgressive magmatism away from the collisional suture, Lithos 344–345 (2019) 265–
479 279, https://doi.org/10.1016/j.lithos.2019.06.031.
480 Ghods, A., Shabanian, E., Bergman, E., Faridi, F., Donner, S., Mortezanejad, G., Aziz-
481 Zanjani, A., 2015. The Varzaghan-Ahar, Iran, Earthquake Doublet 1 (Mw 6.4, 6.2): implications
482 for the geodynamics of northwest Iran. Geophys. J. Int. 203, 522–540. http://dx.doi.org/10.1093/
483 gji/ggv306
484 Goebel, T.H.W., Weingarten, M., Chen, X., Haffener, J., Brodesky, E.E., 2017. The 2016
485 Mw5.1 Fairview, Oklahoma earthquakes: Evidence for long-range poroelastic triggering at >40
486 km from fluid disposal wells, Earth and Planetary Science Letters, 472, 50-61.
487 https://doi.org/10.1016/j.epsl.2017.05.011
488 Harris, R. A. (2017), Large earthquakes and creeping faults, Rev. Geophys., 55, 169-198,
489 doi:10.1002/2016RG000539.
490 Henry, C., & S. Das, 2002. The Mw 8.2 17 February 1996 Biak, Indonesia, earthquake:
491 Rupture history, aftershocks, and fault plane properties, J. Geophys. Res., **107**(B11), 2312, doi:
492 10.1029/2001JB796.
493 Hessami Azar, K., Pantosti, D., Tabassi, H., Shabanian, E., Abbasi, M.R., Feghhi, K.,
494 Solaymani, S., 2003. Paleoearthquakes and slip rates of the North Tabriz Fault, NW Iran:
495 preliminary results. Ann. Geophys. 46, 903–915. DOI: https://doi.org/10.4401/ag-3461
496 Jackson, J., 1992. Partitioning of strike-slip and convergent motion between Eurasia and
497 Arabia in Eastern Turkey and the Caucasus. J. Geophys. Res. 97, 12471–12479.
498 https://doi.org/10.1029/92JB00944
499 Jackson, J., Priestley, K., Berberian, M., 2002. Active tectonics of the South Caspian Basin.
500 Geophys. J. Int. 148, 214–245. https://doi.org/10.1046/j.1365-246X.2002.01588.x

501 Johann, L., Shapiro, S.A. & Dinske, C., 2018. The surge of earthquakes in Central Oklahoma
502 has features of reservoir-induced seismicity. Sci Rep 8, 11505. https://doi.org/10.1038/s41598-
503 018-29883-9.
504 Kagan, Y. Y., and Jackson, D. D., 1991, Long-term earthquake clustering, Geophys. J. Int.,
505 104, 117–133. https://doi.org/10.1111/j.1365-246X.1991.tb02498.x
506 Karakhanian, A., Jrbashyan, R., Trifonov, V., Philip, H., Avagyan, A., Hessami, K., Jamali,
507 Bayraktutan, F. M., Bagdassarian, H., Arakelian, S., Davtyan V., and Adilkhanyan, A., 2004,
508 Active faulting and natural hazards in Armenia, eastern Turkey and Northern Iran,
509 Tectonophysics, 380, 189–219. https://doi.org/10.1016/j.tecto.2003.09.020
510 Khoshmanesh, M., Shirzaei, M., 2018. Episodic creep events on the San Andreas Fault caused
511 by pore pressure variations, Nat. Geosci. https://doi.org/10.1038/s41561-018-0160-2
512 Masson, F., Djamour, Y., Van Gorp, S., Chery, J., Tatar, M., Tavakoli, F., Nankali, H. &
513 Vernant, P., 2006. Extension in NW Iran driven by the motion of the South Caspian Basin, Earth
514 planet. Sci. Lett., 252, 180–188. https://doi.org/10.1016/j.epsl.2006.09.038
515 Michel, S., Avouac, J.P., Jolivet, R., and Wang, L., 2018. Seismic and Aseismic Moment
516 Budget and Implication for the Seismic Potential of the Parkfield Segment of the San Andreas
517 Fault, Bulletin of the Seismological Society of America, Vol. 108, No. 1, pp. 19–38, Doi:
518 10.1785/0120160290.
519 McClusky, S., et al., 2000. Global positioning system constraints on plate kinematics and
520 dynamics in the eastern Mediterranean and Caucasus. J. Geophys. Res. 105, 5695–5719.
521 https://doi.org/10.1029/1999JB900351
522 Momeni, S.M., Tatar, M., 2018. Mainshocks/aftershocks study of the August 2012 earthquake
523 doublet on Ahar-Varzaghan complex fault system (NW Iran). Physics of the Earth and Planetary

Interiors, **283**, 67-81. https://doi.org/10.1016/j.pepi.2018.08.001

Momeni, S.M., Aoudia, A., Tatar, M., Twardzik, C. & Madariaga, R., 2019. Kinematics of the 2012 Ahar–Varzaghan complex earthquake doublet ($M_w$6.5 and $M_w$6.3), *Geophysical Journal International*, **217**, 2097–2124, https://doi.org/10.1093/gji/ggz100

Momeni, S.M., Madariaga, R., 2020. Long-term induced seismicity on the Mosha fault by Damavand Volcano, N-Iran, Implications on the seismic hazard of Tehran metropolis, under review in SRL.

Moradi, A.S., Hatzfeld, D. & Tatar, M., 2011. Microseismicity and seismotectonics of the North Tabriz Fault (Iran), Tectonophysics, 506, 22–30. https://doi.org/10.1016/j.tecto.2011.04.008

Noda, H., & Lapusta, N., 2013, Stable creeping fault segments can become destructive as a result of dynamic weakening, NATURE, **493**, 518-521, doi:10.1038/nature11703

Schulz, S., Darehshouri, S., Hassanzadeh, E. et al. 2020. Climate change or irrigated agriculture – what drives the water level decline of Lake Urmia. Sci Rep 10, 236. https://doi.org/10.1038/s41598-019-57150-y.

Su, Z., Wang, E., Hu, J., Talebian, M. & Karimzadeh, S., (2017). Quantifying the Termination Mechanism Along the North Tabriz-North Mishu Fault Zone of Northwestern Iran via Small Baseline PS-InSAR and GPS Decomposition. IEEE Journal of Selected Topics in Applied Earth Observations and Remote Sensing, vol. 10, no. 1, pp. 130-144, doi: 10.1109/JSTARS.2016.2586742.

Reilinger, R., et al., 2006. GPS constraints on continental deformation in the Africa- Arabia-Eurasia continental collision zone and implications for the dynamics of plate interactions. J. Geophys. Res. 111, B05411. https://doi.org/10.1029/2005JB004051.

547 Rezaeifar, M., Kissling, E., Shomali, Z.H. & Shahpasand-Zadeh, M., 2016. 3D crustal
548 structure of the northwest Alborz region (Iran) from local earthquake tomography. Swiss J.
549 Geosci., 1–12, Springer International Publishing. doi:10.1007/s00015-016-0219-2
550 Rizza, M., Vernant, P., Ritz, J., Peyrat, M., Nankali, H., Nazari, H., Djamour, Y., Salamati,
551 R., Tavakoli, F., Chéry, J., Mahan, S., Masson, F., 2013. Morphotectonic and geodetic evidence
552 for a constant slip-rate over the last 45 kyr along the Tabriz fault (Iran). Geophys. J. Int. 193,
553 1083–1094. https://doi.org/10.1093/gji/ggt041
554 Ruiz, S., & Madariaga, R., 2013. Kinematic and dynamic inversion of the 2008 northern
555 Iwate earthquake, Bull. Seismol. Soc. Am., **103**(2A), 694–708, Doi: 10.1785/0120120056.
556 Saar, M.O., Manga, M., 2003. Seismicity induced by seasonal groundwater recharge at Mt.
557 Hood, Oregon, Earth and Planetary Science Letters, 214, 605-618.
558 https://doi.org/10.1016/S0012-821X(03)00418-7
559 Scuderi, M.M., Collettini, C., Marone, C., 2017. Frictional stability and earthquake triggering
560 during fluid pressure stimulation of an experimental fault, Earth and Planetary Science Letters,
561 **477**, 84-96. https://doi.org/10.1016/j.epsl.2017.08.009
562 Solaymani Azad, S., Philip, H., Dominguez, S., Hessami Azar, K., Shahpasandzadeh, M.,
563 Foroutan, M., Tabassi, H., Lamothe, M., 2015. Paleoseismological and morphological evidence
564 of slip rate variations along the North Tabriz fault (NW Iran). Tectonophysics, 640–641, 20-38.
565 https://doi.org/10.1016/j.tecto.2014.11.010
566 Van den Ende, M.P.A., Chen, J., Ampuero J.P. & Niemeijer A.R., 2020. Rheological
567 Transitions Facilitate Fault−Spanning Ruptures on Seismically Active and Creeping Faults,
568 Journal of Geophysical Research: Solid Earth Volume 125, Issue 8,
569 https://doi.org/10.1029/2019JB019328

570 Vadacca, L., 2020, The Altotiberina Low-Angle Normal Fault (Italy) Can Fail in Moderate-
571 Magnitude Earthquakes as a Result of Stress Transfer from Stable Creeping Fault Area,
572 Geosciences, 10, 144; doi:10.3390/geosciences10040144.
573 Valerio, E., Manzo, M., Casu, F., Convertito, V., De Luca, C., Manunta, M., Monterroso, F.,
574 Lanari, R. & De Novellis, V., 2020. Seismogenic Source Model of the 2019, Mw 5.9, East-
575 Azerbaijan Earthquake (NW Iran) through the Inversion of Sentinel-1 DInSAR Measurements,
576 Remote Sens., 12, 1346; doi:10.3390/rs12081346.
577 Vernant, Ph., et al., 2004. Contemporary crustal deformation and plate kinematics in Middle
578 East constrained by GPS measurements in Iran and northern Oman. Geophys. J. Int. 157, 381–
579 398.
580 Wang, R., Martin, F.L., Roth, F., (2003). Computation of deformation induced by earthquakes
581 in a multi-layered elastic crust—FORTRAN programs EDGRN/EDCM, Computers &
582 Geosciences 29, 195–207, 2003.
583 Zamani, B., Masson, F., 2014. Recent tectonics of East (Iranian) Azerbaijan from stress state
584 reconstructions. Tectonophysics 611, 61–82.
585 Zhu, W., Allison, K.L., Dunham, E.M., Yang, Y., 2020. Fault Valving and Pore Pressure
586 Evolution in Simulations of Earthquake Sequences and Aseismic Slip, Computational Physics,
587 https://arxiv.org/abs/2001.03852.
588

589 **Mailing address:**

590 Seyyedmaalek Momeni
591 EPFL Geo-Energy Lab – Gaznat Chair on Geo-Energy, EPFL-ENAC-IIC-GEL, Station 18, CH-
592 1015, Lausanne, Switzerland.

**Figure Captions:**

**Figure 1**. (**a**) Seismotectonics of the study region. Stars show the 2012 AVD hypocenter locations, and the related focal mechanisms are by Momeni & Tatar, (2018). Faults are in lines. Vectors are geodetic surface deformation rates by Masson et al., (2006), fixing the central Iran block. Hexagons are historical earthquakes (Ambraseys & Melvile, 1982; Berberian & Yeats, 1999, 2001). Circles are instrumental earthquakes by Engdahl et al. (2006). Dashed ellipses show affected regions by the 1593, 1721, 1780, and 1786 historical earthquakes. Fault names are: ASF: Astaneh, WAF: West Alborz, SQF: South Qoshadagh, GCF: Goshachay, NBF: North Bozkosh, SBF: South Bozkosh, NMF: North Mishu, SMF: South Mishu, MGF: Maraghe, NKH: Nakhjavan, KHF: Khajeh, and NHF: Nehram. NTF is in thick solid line. (**b**) Circles: Seismicity recorded in IRSC network from 2006 until before the AVD. Colors represent hypocentral depths. Faults are the same as (a). Focal mechanisms with label are from the GCMT catalog until August 2020. Those labeled M6.1 ARD, M6.5 AVD1, M6.3 AVD2, and M5.9 TKC are from the 1997 Ardebil, 2012 AVD doublet and 2019 Mw5.9 Torkamanchay earthquakes. Triangles are the Tabriz permanent seismic sub-network stations belong to IRSC.

**Figure 2**. Seismicity along NTF and NMF. (**a**): black circles are the earthquakes from 2006 to before the 2012 AVD and white circles are the earthquakes that occurred after 2012 AVD until 2019 TKC. Ellipse is the estimated cumulative slip model for the creeping segment of NTF near SND from 1721 AD historical earthquake until AVD. The dashed circle is the thermal area (after Ghalamghash et al, 2019). (**b**) up: histogram showing seismicity selected in distance of 5 km

615 from NTF and NMF shown in (a). NMF stands for North Mishu Fault. down: Diagram of
616 cumulative scalar seismic moments along NTF and NMF.
617
618 **Figure 3**. Transferred Coulomb stress field from the creeping segment of NTF on the (**a**) AVD
619 ruptures and (**b**) the Western and Eastern segments of the creep segment of NTF, where high
620 seismic activity was observed. The shown Coulomb stress fields are for the depth of 6 km.
621 Circles along NTF are earthquakes from 2006 until AVD. The rest are early aftershocks of the
622 AVD (IRSC). Dashed circle is the thermal area by Ghalamghash et al., (2019). Solid large circle
623 shows the area of neo-Sahand young craters near Bostan Abad (BA). Dashed line marked A is
624 the position of vertical cross sections shown in Figures 5 and 6.
625
626 **Figure 4**. (**a**): Transferred Coulomb stress fields from AVD ruptures on NTF (up: EV#1, down:
627 EV#2). (**b**): Transferred Normal stress fields from AVD ruptures on NTF (up: EV#1, down:
628 EV#2). The shown stress fields are for the depth of 10 km.
629
630 **Figure 5.** Schematic plot illustrating the relation between SND magmatic activity, NTF creeping
631 segment, and AVD ruptures (marked AV#1 & AV#2). Low and high velocity areas are from
632 Bavali et al., (2016), Rezaeifar et al., (2016), and Ghalamghash et al, (2019) studies. Stars are the
633 11 August 2012 M6.5&M6.3 mainshocks centroids. Thick dashed line is the NTF. Horizontal
634 dashed lines are crustal velocity layers from Momeni & Tatar, (2018).
635
636 **Figure 6.** Graphic illustration of triggering of the 2012 AVD by the transfer of Coulomb stress
637 field produced by the central NTF creeping segment. Stars are the mainshocks hypocenters.

Rupture models are from Momeni et al., (2019). Horizontal dashed lines are crustal velocity layers from Momeni & Tatar, (2018).

**Figures:**

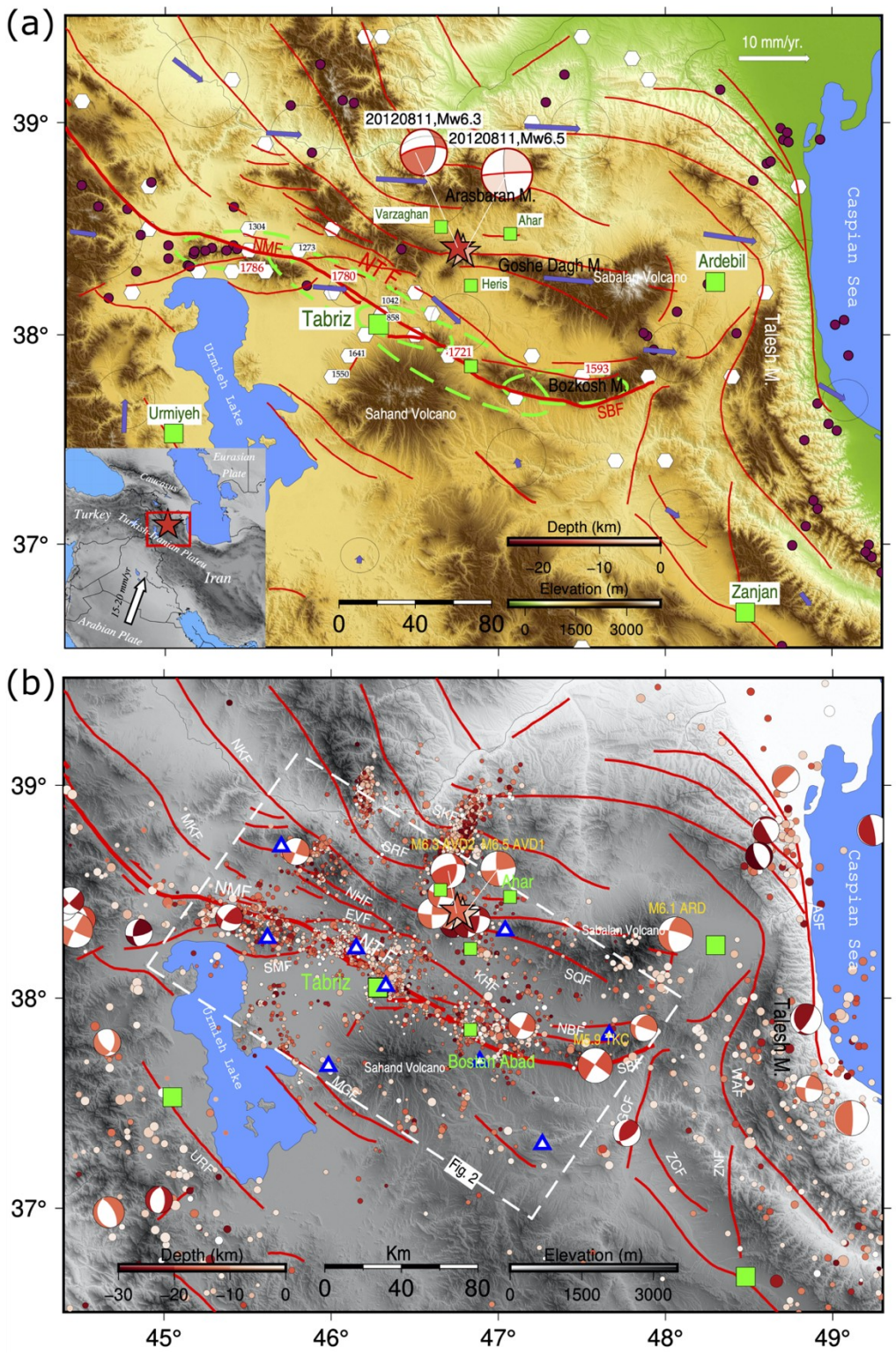


643

644 **Figure 1**. (**a**) Seismotectonics of the study region. **(b)** Seismicity recorded in IRSC network from

645 2006 until before the AVD.

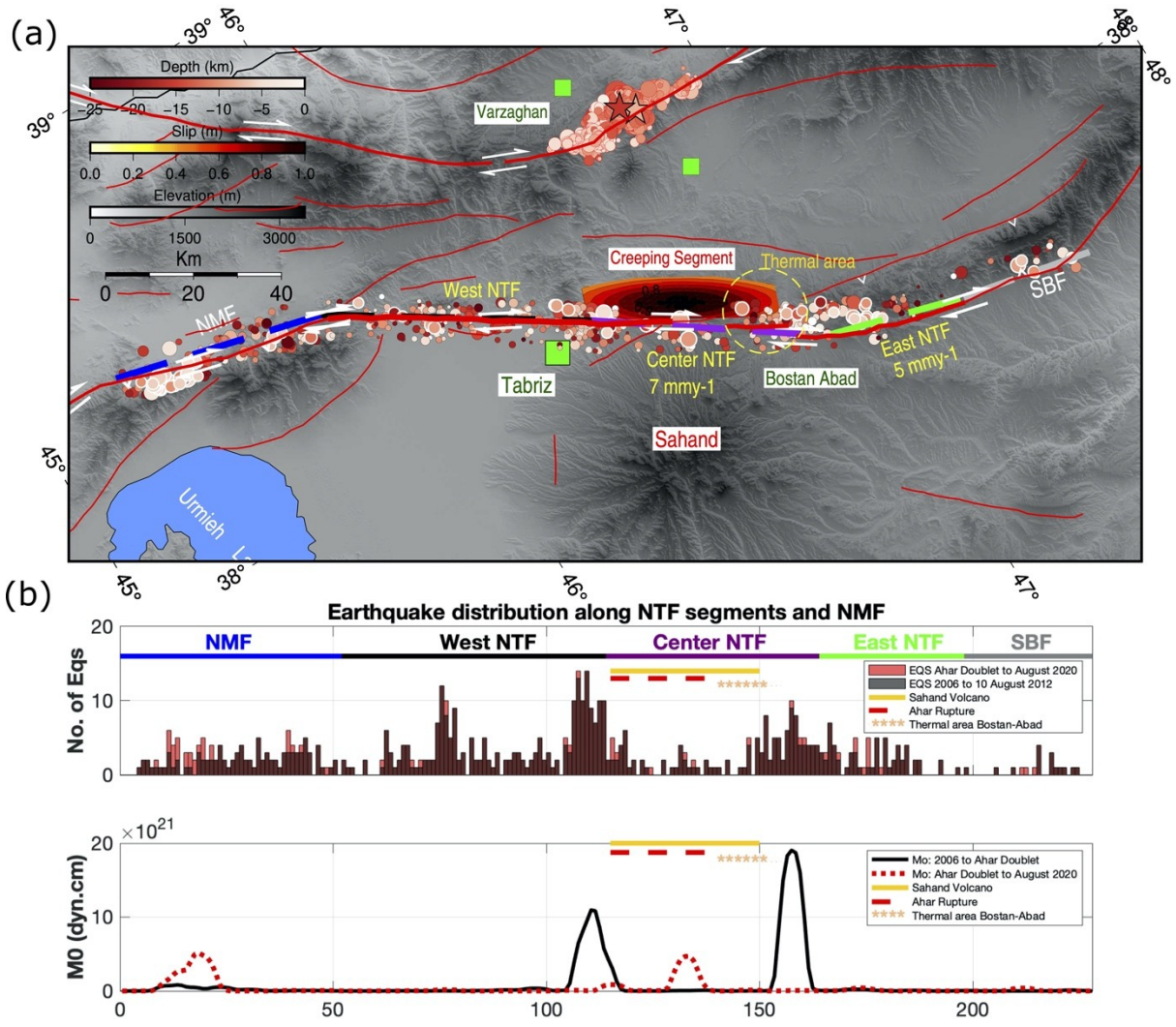


**Figure 2**. **(a)** Seismicity along NTF and NMF. **(b)** Histograms of earthquake distribution along NTF and NMF.

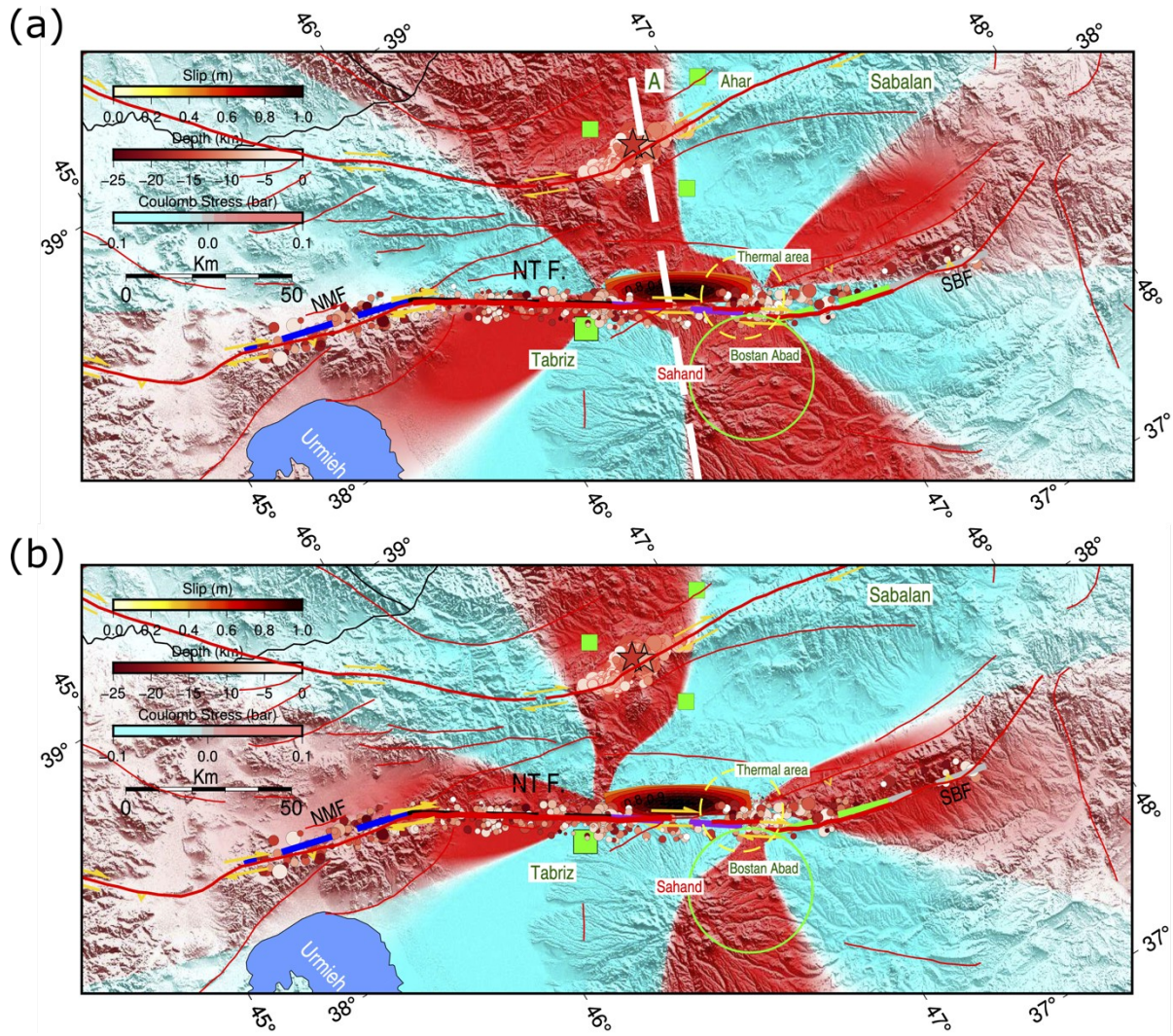


**Figure 3**. Transferred Coulomb stress field from the creeping segment of NTF. **(a)** on the AVD ruptures and **(b)** on the Western and Eastern segments of the creeping segment.

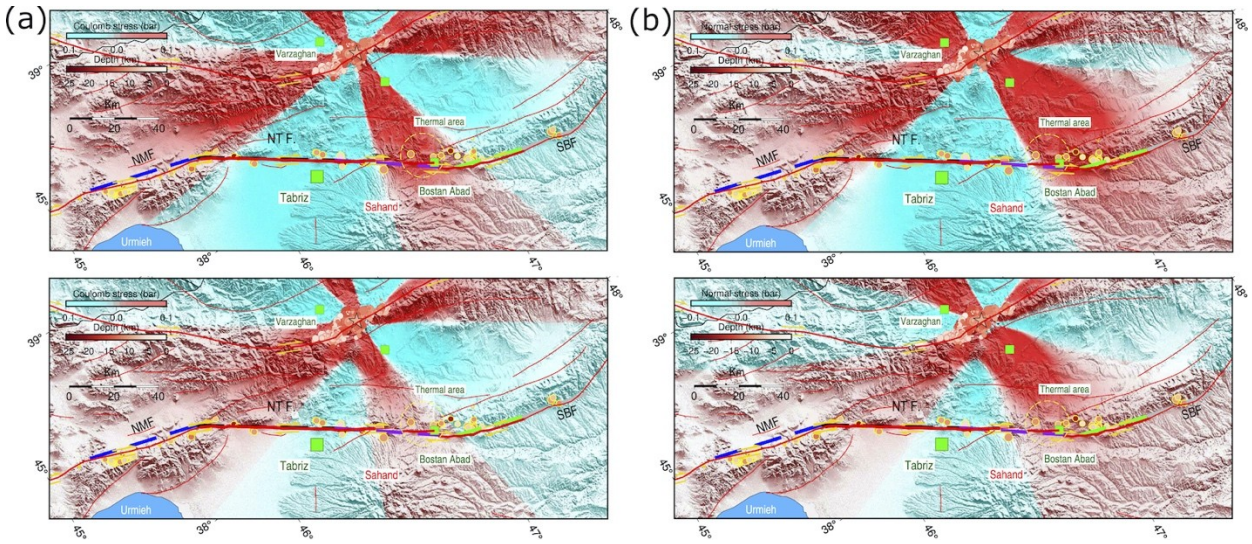


**Figure 4**. Transferred **(a)** Coulomb and **(b)** Normal stress fields from AVD ruptures on NTF.

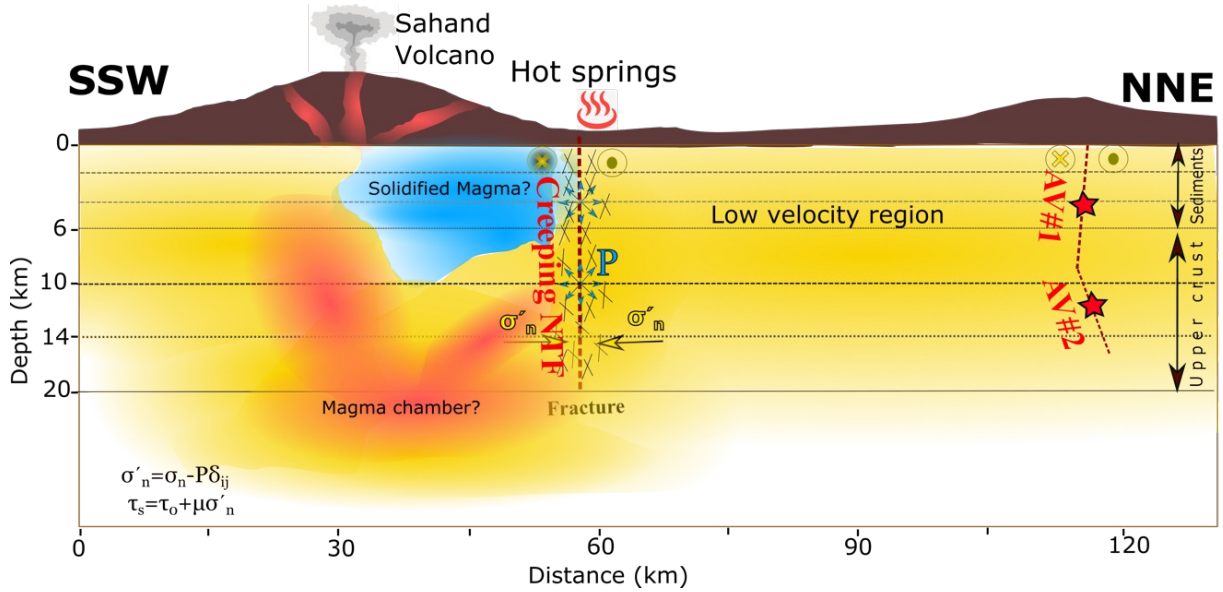


665

666 **Figure 5**. Schematic plot illustrating the relation between SND magmatic activity, NTF

667 creeping segment, and AVD ruptures.

668

669

670

671

672

673

674

675

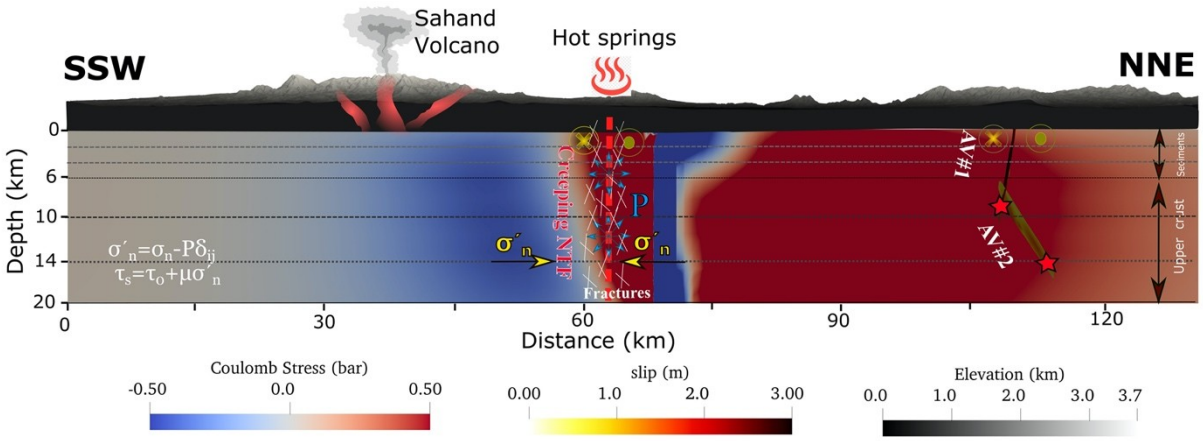


**Figure 6**. Graphic illustration of triggering of the 2012 AVD by the transfer of Coulomb stress field produced by the central NTF creeping segment.

**Electronic Supplement**

**Tables:**

**Table S1.** Velocity model of the NW Iran by Momeni & Tatar, (2018).

| Depth of layer top | Vp | Vs |
|---|---|---|
| -3 | 4.58 | 2.44 |
| 2 | 5.65 | 3.11 |
| 4 | 5.92 | 3.34 |
| 6 | 6.20 | 3.53 |
| 10 | 6.35 | 3.63 |
| 14 | 6.52 | 3.71 |
| 46 | 8.10 | 4.63 |

**Table S2. Earthquakes with Ml>=2.5 along the North Tabriz fault segments and NMF and SBF from 2006 until before the August 2012 Ahar-Varzaghan earthquake doublet (Mw6.5&6.3) (IRSC).**

| | Longitude | Latitude | Year | Month | Day | Magnitude | Depth | Hour | Minute |
|---|---|---|---|---|---|---|---|---|---|
| **Central NTF** | 46.56 | 37.95 | 2007 | 10 | 4 | 2.7 | 12.80 | 3 | 2 |
| | 46.43 | 38.09 | 2007 | 12 | 1 | 4.5 | 7.4 | 18 | 45 |
| | 46.64 | 37.94 | 2008 | 3 | 24 | 3.1 | 11.8 | 9 | 44 |
| | 46.42 | 38.10 | 2008 | 4 | 7 | 3.2 | 11.4 | 2 | 48 |
| | 46.42 | 38.09 | 2008 | 5 | 10 | 3.3 | 15.1 | 16 | 15 |
| | 46.57 | 37.96 | 2009 | 6 | 13 | 2.7 | 15.5 | 23 | 21 |
| | 46.82 | 37.87 | 2009 | 10 | 12 | 2.7 | 9.8 | 20 | 55 |
| | 46.84 | 37.86 | 2010 | 2 | 2 | 3.6 | 5.0 | 10 | 5 |
| | 46.84 | 37.83 | 2010 | 2 | 2 | 3.4 | 2.1 | 10 | 15 |
| | 46.84 | 37.86 | 2010 | 2 | 2 | 4.6 | 5.0 | 10 | 16 |
| | 46.83 | 37.84 | 2010 | 2 | 2 | 3.8 | 5.0 | 11 | 26 |
| **Eastern NTF** | 47.21 | 37.72 | 2006 | 2 | 2 | 2.9 | 8.4 | 19 | 49 |
| | 46.99 | 37.81 | 2007 | 5 | 26 | 2.5 | 8.4 | 22 | 1 |
| | 47 | 37.73 | 2007 | 6 | 21 | 2.7 | 3.5 | 16 | 27 |
| | 46.97 | 37.82 | 2008 | 1 | 28 | 2.8 | 5.4 | 13 | 38 |
| | 47.13 | 37.73 | 2008 | 4 | 19 | 3.1 | 18 | 13 | 36 |
| | 46.88 | 37.84 | 2010 | 2 | 2 | 3.0 | 11.6 | 13 | 23 |
| | 47.04 | 37.77 | 2011 | 10 | 18 | 2.9 | 1.7 | 21 | 4 |
| **Western NTF** | 46.22 | 38.20 | 2006 | 1 | 8 | 3.1 | 4.0 | 17 | 19 |
| | 46.34 | 38.07 | 2008 | 1 | 22 | 2.5 | 10 | 8 | 55 |
| | 46.34 | 38.14 | 2008 | 6 | 1 | 2.6 | 13.50 | 2 | 17 |
| | 46.18 | 38.16 | 2008 | 6 | 26 | 2.6 | 16.20 | 16 | 34 |
| | 46.20 | 38.15 | 2008 | 6 | 26 | 2.6 | 14.70 | 16 | 39 |
| | 46.18 | 38.16 | 2008 | 6 | 26 | 3.1 | 16.70 | 17 | 6 |
| | 46.18 | 38.16 | 2008 | 6 | 26 | 2.7 | 15.80 | 17 | 8 |
| | 46.35 | 38.13 | 2008 | 7 | 28 | 2.9 | 17.20 | 7 | 13 |
| | 46.10 | 38.23 | 2009 | 2 | 13 | 2.6 | 5.1 | 4 | 0 |
| | 46.39 | 38.11 | 2009 | 8 | 5 | 2.6 | 10.40 | 22 | 15 |
| | 45.93 | 38.29 | 2010 | 1 | 4 | 2.6 | 10 | 7 | 38 |
| | 46.34 | 38.12 | 2011 | 1 | 29 | 3 | 14.80 | 7 | 29 |
| | 46.36 | 38.10 | 2012 | 5 | 4 | 2.6 | 7.8 | 21 | 48 |
| **NMF** | 45.47 | 38.41 | 2006 | 8 | 12 | 3.6 | 13.60 | 7 | 2 |
| | 45.35 | 38.49 | 2007 | 7 | 8 | 2.6 | 15.80 | 22 | 49 |
| | 45.38 | 38.40 | 2008 | 4 | 22 | 3.7 | 9 | 19 | 53 |
| | 45.74 | 38.34 | 2008 | 9 | 6 | 2.6 | 3 | 11 | 8 |
| | 45.41 | 38.47 | 2009 | 4 | 24 | 3.6 | 3.8 | 18 | 28 |
| | 45.45 | 38.39 | 2011 | 8 | 19 | 2.6 | 19.8 | 4 | 31 |
| | 45.69 | 38.36 | 2012 | 2 | 5 | 2.9 | 23.6 | 22 | 15 |
| | 45.57 | 38.43 | 2012 | 4 | 29 | 3.2 | 8 | 0 | 16 |
| | 45.55 | 38.42 | 2012 | 4 | 29 | 3 | 11.20 | 0 | 22 |
| **SBF** | 47.55 | 37.64 | 2008 | 6 | 12 | 2.5 | 10 | 3 | 19 |
| | 47.29 | 37.75 | 2010 | 7 | 14 | 2.9 | 18 | 16 | 46 |
| | 47.54 | 37.68 | 2010 | 10 | 23 | 2.7 | 4.10 | 17 | 59 |
| | 47.55 | 37.66 | 2011 | 6 | 6 | 3.1 | 0.70 | 12 | 23 |
| | 47.55 | 37.64 | 2008 | 6 | 12 | 2.5 | 10 | 3 | 19 |

693
694

**Table S3. Earthquakes with Ml>=2.5 along the North Tabriz fault segments and NMF and SBF from the August 2012 Ahar-Varzaghan earthquake doublet until the November 2019 Mw5.9 Torkamanchay earthquake (IRSC).**

| | Longitude | Latitude | Year | Month | Day | Magnitude | Depth | Hour | Minute |
|---|---|---|---|---|---|---|---|---|---|
| **Central NTF** | 46.47 | 38.06 | 2012 | 12 | 13 | 2.7 | 18 | 0 | 29 |
| | 46.75 | 37.93 | 2012 | 12 | 16 | 3.2 | 10 | 10 | 41 |
| | 46.42 | 38.09 | 2014 | 3 | 9 | 3.6 | 7.4 | 6 | 34 |
| | 46.59 | 37.93 | 2015 | 1 | 19 | 3.8 | 9.5 | 11 | 53 |
| | 46.84 | 37.87 | 2015 | 12 | 2 | 2.8 | 8 | 0 | 31 |
| | 46.52 | 38.00 | 2016 | 1 | 27 | 3.0 | 14.7 | 20 | 31 |
| | 46.43 | 38.04 | 2016 | 6 | 27 | 2.5 | 19.6 | 18 | 38 |
| | 46.42 | 38.03 | 2017 | 1 | 5 | 2.6 | 5.7 | 4 | 33 |
| | 46.43 | 38.06 | 2018 | 12 | 12 | 3.5 | 6 | 5 | 56 |
| | 46.44 | 38.07 | 2018 | 12 | 21 | 3.6 | 5 | 9 | 39 |
| | 46.60 | 37.98 | 2019 | 8 | 16 | 4.2 | 8.9 | 10 | 55 |
| **Eastern NTF** | 47.03 | 37.80 | 2013 | 2 | 8 | 2.6 | 10 | 19 | 25 |
| | 46.95 | 37.82 | 2013 | 2 | 12 | 2.5 | 5.1 | 8 | 11 |
| | 47.05 | 37.76 | 2014 | 2 | 11 | 2.7 | 5.4 | 10 | 18 |
| | 47.04 | 37.77 | 2014 | 8 | 19 | 2.5 | 10 | 5 | 43 |
| | 47.02 | 37.78 | 2014 | 9 | 8 | 2.8 | 10 | 16 | 53 |
| | 47.04 | 37.80 | 2018 | 6 | 1 | 2.5 | 10 | 0 | 8 |
| | 46.99 | 37.79 | 2018 | 11 | 24 | 3.3 | 8.6 | 17 | 22 |
| | 47.01 | 37.78 | 2018 | 11 | 25 | 2.5 | 10 | 9 | 46 |
| | 47.00 | 37.78 | 2018 | 11 | 26 | 3.3 | 6 | 20 | 9 |
| | 46.99 | 37.79 | 2018 | 11 | 27 | 2.7 | 6 | 11 | 33 |
| **Western NTF** | 45.89 | 38.29 | 2013 | 10 | 12 | 2.9 | 6 | 5 | 48 |
| | 45.90 | 38.35 | 2015 | 2 | 5 | 2.5 | 6.9 | 7 | 40 |
| | 46.38 | 38.13 | 2015 | 4 | 4 | 2.8 | 10 | 21 | 24 |
| | 45.97 | 38.30 | 2016 | 10 | 28 | 2.7 | 19.3 | 9 | 18 |
| | 46.31 | 38.07 | 2016 | 11 | 14 | 3.6 | 7.6 | 3 | 35 |
| | 45.98 | 38.28 | 2016 | 12 | 29 | 2.6 | 10 | 8 | 36 |
| | 46.34 | 38.12 | 2017 | 3 | 31 | 2.7 | 10 | 20 | 4 |
| | 46.32 | 38.07 | 2017 | 6 | 23 | 2.6 | 8 | 4 | 35 |
| | 46.04 | 38.23 | 2018 | 1 | 22 | 3.2 | 8.4 | 15 | 59 |
| | 46.04 | 38.23 | 2018 | 1 | 22 | 2.9 | 9.4 | 16 | 14 |
| | 46.34 | 38.14 | 2018 | 5 | 6 | 2.7 | 9.4 | 8 | 33 |
| | 46.36 | 38.11 | 2018 | 6 | 22 | 2.9 | 10 | 17 | 5 |
| | 46.34 | 38.13 | 2019 | 5 | 8 | 2.9 | 8.9 | 22 | 57 |
| **NMF** | 45.36 | 38.43 | 2013 | 4 | 18 | 4.9 | 6.1 | 10 | 39 |
| | 45.34 | 38.41 | 2013 | 4 | 18 | 3 | 10.2 | 10 | 53 |
| | 45.35 | 38.42 | 2013 | 4 | 18 | 2.9 | 12 | 11 | 32 |
| | 45.38 | 38.41 | 2013 | 4 | 18 | 3.9 | 6.4 | 11 | 40 |
| | 45.33 | 38.42 | 2013 | 4 | 18 | 2.6 | 30.3 | 13 | 30 |
| | 45.39 | 38.40 | 2013 | 4 | 29 | 2.6 | 12.6 | 14 | 36 |
| | 45.41 | 38.40 | 2013 | 6 | 28 | 4.2 | 5.30 | 5 | 13 |

| | | | | | | | | | |
|---|---|---|---|---|---|---|---|---|---|
| | 45.46 | 38.45 | 2014 | 3 | 12 | 2.6 | 10.8 | 10 | 28 |
| | 45.60 | 38.43 | 2014 | 5 | 13 | 2.5 | 9.8 | 3 | 59 |
| | 45.30 | 38.44 | 2015 | 4 | 10 | 2.5 | 10 | 19 | 17 |
| | 45.75 | 38.34 | 2015 | 12 | 31 | 3 | 11.8 | 22 | 31 |
| | 45.65 | 38.37 | 2016 | 2 | 15 | 2.5 | 7.3 | 4 | 56 |
| | 45.67 | 38.39 | 2016 | 9 | 26 | 2.5 | 8 | 20 | 35 |
| | 45.71 | 38.35 | 2016 | 9 | 27 | 3.7 | 5 | 18 | 18 |
| | 45.67 | 38.38 | 2016 | 10 | 7 | 2.6 | 4 | 7 | 13 |
| | 45.40 | 38.40 | 2016 | 12 | 26 | 2.9 | 18.3 | 1 | 55 |
| | 45.34 | 38.41 | 2017 | 12 | 4 | 2.5 | 7 | 7 | 0 |
| | 45.37 | 38.43 | 2018 | 1 | 13 | 3.2 | 6 | 0 | 50 |
| | 45.69 | 38.38 | 2018 | 3 | 4 | 2.6 | 6 | 8 | 16 |
| | 45.33 | 38.41 | 2018 | 3 | 30 | 2.7 | 4 | 10 | 10 |
| | 45.40 | 38.41 | 2018 | 4 | 30 | 3.4 | 11 | 5 | 49 |
| | 45.66 | 38.38 | 2018 | 6 | 19 | 2.6 | 9 | 2 | 56 |
| | 45.66 | 38.38 | 2018 | 9 | 4 | 2.6 | 6.4 | 1 | 50 |
| | 45.42 | 38.41 | 2018 | 11 | 21 | 3.3 | 5 | 0 | 42 |
| | 45.45 | 38.42 | 2018 | 12 | 26 | 3.5 | 5 | 7 | 41 |
| | 45.33 | 38.42 | 2019 | 4 | 11 | 2.7 | 10 | 9 | 14 |
| | 45.33 | 38.42 | 2019 | 4 | 12 | 3.4 | 6 | 0 | 16 |
| | 45.35 | 38.43 | 2019 | 4 | 12 | 3.8 | 6 | 4 | 12 |
| | 45.33 | 38.43 | 2019 | 4 | 12 | 2.7 | 6 | 6 | 14 |
| | 45.39 | 38.40 | 2019 | 6 | 8 | 2.8 | 6 | 0 | 54 |
| | 45.44 | 38.39 | 2019 | 6 | 8 | 2.5 | 6 | 1 | 0 |
| | 45.44 | 38.43 | 2019 | 6 | 9 | 2.8 | 4.9 | 4 | 14 |
| **SBF** | 47.47 | 37.67 | 2013 | 1 | 15 | 2.7 | 13.1 | 5 | 31 |
| | 47.42 | 37.71 | 2015 | 12 | 28 | 3.5 | 9 | 10 | 3 |
| | 47.44 | 37.71 | 2019 | 4 | 15 | 2.7 | 6.8 | 6 | 22 |

699